CHEMISTRY JOURNAL OF MOLDOVA. General, Industrial and Ecological Chemistry. 2024, 19(1), 102-111
ISSN (p) 1857-1727 ISSN (e) 2345-1688
http://cjm.ichem.md
https://doi.org/10.19261/cjm.2024.1157

ENHANCING DSSC PERFORMANCE THROUGH CHLOROPHYLL AND PORPHYRIN DYE INCORPORATION ON TiO_2-ZnO: Al COMPOSITES

Sri Wuryanti*, Tina Mulya Gantina, Annisa Syafitri Kurniasetiawati

Department of Energy Conversion Engineering, Politeknik Negeri Bandung, Jl. Gegerkalong Hilir, Desa Ciwaruga, Kecamatan Parongpong, Kabupaten Bandung Barat 40559, Indonesia
**e-mail: sriwuryanti.lamda@gmail.com*

Abstract. This research systematically investigates the impact of porphyrin and chlorophyll dyes on Dye-Sensitized Solar Cells (DSSC) performance, aims to achieve maximum solar cell efficiency. This investigation involved the use of Fluorine-doped Tin Oxide (FTO) coating with TiO_2–ZnO composite, incorporating Al doping, and introducing variations in the concentration of chlorophyll SP and porphyrin (2:2:0.1 and 2:2:0.2). Synthesis of Al-doped ZnO was carried out via the sol-gel method, which involves mixing and heating at 65°C, followed by degradation at 150°C. TiO_2 and ZnO: Al composites were formed using the sonication method at 45°C for 60 minutes. This study evaluates the impact of dyes on the growth of TiO_2 and ZnO: Al composites and examines their characteristics - including UV-Vis, band gap, current versus voltage curves, DSSC efficiency-using EDX, and FTIR analyses of solar cells. The DSSC efficiency testing utilizes a photon light source from a halogen lamp with an intensity of 328-580 lux. The results showed that DSSC based on TiO_2–ZnO: Al + chlorophyll produced an efficiency of 13.3%, while porphyrin (2:2:0.1) and (2:2:0.2) produced an efficiency of 8.9% and 13.9%, respectively. In conclusion, this study shows that adding dye to the TiO_2–ZnO: Al composite significantly improves DSSC performance and shows optimal characteristics. The highest DSSC efficiency of 13.9% underscores the interdependence of absorber layer quality with photovoltaic performance, providing valuable insights for future solar cell design and optimization.

Keywords: TiO_2 and ZnO fluorine-doped tin oxide, porphyrin, ZnO with Al doping.

Received: 15 March 2024/ Revised final: 04 June 2024/ Accepted: 06 June 2024

Introduction

Solar cells operate on the fundamental principle of photovoltaic, harnessing the ability to convert light into electrical energy. The generation of Dye-Sensitized Solar Cells (DSSC) has significant advances in the field of solar cell materials [1]. DSSC efficiency has demonstrated remarkable progress, achieving levels of 11% [2] and 12.3% [3], particularly when utilizing TiO_2 as the active material in the working electrode.

Recent advancements have shown that employing SM315 porphyrin dye [4] with TiO_2 as the semiconductor can further enhance power conversion efficiency, reaching an impressive 13%. Despite TiO_2's efficiency as a photo-catalyst [5-10], its limited surface area poses a challenge, resulting in relatively low adsorption of the photo-catalyst. Additionally, the higher cost of TiO_2, compared to ZnO, has led researchers to explore ZnO as a viable alternative for the working electrode [11-15]. ZnO, an abundant natural element with an energy gap of 3.37 eV, is a justifiable substitute given its energy characteristics comparable to TiO_2 (3.2 eV) [16].

Various materials, such as Ga, Sn, Mg, Al, and B, have been explored for doping to further optimize ZnO's physical, optical, and electrical properties [17]. Aluminium is a convenient choice for atomic doping [18-22] due to its smaller ionic radius compared to ZnO, which enhances the electrical conductivity of ZnO and presents a cost-effective alternative to other materials [23,24].

Considering these factors, the combination of TiO_2 with ZnO emerges as a necessity for developing components with superior optical and electrical properties for photo-electronic applications [25]. This study introduces innovation by focusing on the composite TiO_2–ZnO with Al doping [26]. The sol-gel method, involving forming initial compounds (precursors) followed by drying and calcination, is employed for doping ZnO with Al. Additionally, the sonication method, utilizing ultrasonic waves with a frequency of 20 kHz – 10 MHz, is adopted for manufacturing TiO_2–ZnO: Al composites specifically tailored for solar cell applications.

Since TiO_2 exhibits absorbance primarily in ultraviolet wavelengths, incorporating a sensitizer becomes imperative to extend its absorption spectrum into the visible light range [27]. The objective of this study is to investigate the enhancement of sensitivity and efficiency through the utilization of porphyrin dye and chlorophyll extracted from *Syzygium Paniculatum* (S.P.) as sensitizers. The study aims to comprehensively compare the performance of these two sensitizers in enhancing sensitivity and efficiency.

Experimental

Materials

This study utilized TiO_2, ZnO, $AlCl_3$, Al-doped ZnO, methanol, ethanol, NaOH, distilled water, iodine, KI, ethylene glycol (EG), carbon, chlorophyll from S.P. and porphyrin produced by HACH, Germany (Hach Method 8143 Range: 2–210 μg/L Cu).

Al-doped ZnO synthesis process via the sol-gel method

The materials used included ZnO, methanol as a solvent, NaOH as a ligand, hexane for washing, and aluminium trichloride ($AlCl_3$) as a dopant compound. One hundred grams of ZnO and 80 mL of methanol were heated on a hotplate with a stirrer at 60°C for 15 minutes, resulting in percussion. Separately, one hundred grams of $AlCl_3$ and 50 grams of NaOH were dissolved in 200 mL methanol and heated on a hotplate with a stirrer at 60°C for 15 minutes. The heating percussion was carried out using a three-neck flask by slowly dripping the NaOH + $AlCl_3$ + MeOH solution. Stirring continued at 65°C for 180 minutes until the solution turned white. The solution was then allowed to stand for 48 hours until a white precipitate formed. The resultant mixture was washed with 10 mL hexane and 10 mL methanol to produce ZnO, which was then dried in an oven at 150°C for 8 hours, producing ZnO powder [28-30].

Mixing TiO_2, ZnO: Al, and chlorophyll dye using the sonication method

The materials used were nano TiO_2, Al-doped ZnO, ethanol as a solvent, and distilled water. The process involved mixing with several variations and operating conditions at a temperature of 45°C, 70% amplitude on-off for 20 minutes, as follows [31,32].

TiO_2 powder (20 g), distilled water (15 mL), and (EG) (15 mL) were sonicated for 20 minutes until TiO_2 was entirely dispersed. An addition of 20 g of ZnO: Al was re-sonicated for 20 minutes, and 10 mL of chlorophyll was added and sonicated again for 20 minutes (TiO_2–ZnO: Al + chlorophyll composite).

TiO_2 powder (20 g), distilled water (15 mL), and EG (15 mL) were sonicated for 20 minutes until TiO_2 was entirely dispersed. An addition of 20 g of ZnO: Al was re-sonicated for 20 minutes, 1 mg of porphyrin was added and sonicated again for 20 minutes (TiO_2–ZnO: Al + porphyrin 2: 2: 0.1 composite).

TiO_2 powder (20 g), distilled water (15 mL), and EG (15 mL) were sonicated for 20 minutes until TiO_2 was entirely dispersed. An addition of 20 g ZnO: Al was re-sonicated for 20 minutes, and 2 mg of chlorophyll was added and sonicated again for 20 minutes (TiO_2–ZnO: Al + porphyrin 2: 2: 0.2 composite).

FTO coating with TiO_2-ZnO composite doped with Al and dye using a spray gun for solar cell materials

The FTO was cleaned using ethanol, and the process of deposition of the initiator layer (seed layer) on top of the FTO substrate was performed. The seed layer solution consists of TiO_2, ZnO: Al + dye. Layer deposition was performed using a pressurized gun spray technique at 3.2 kg/cm^2. The heating process was gradual, starting at 150°C and increasing to 250°C, aimed at facilitating the formation of the TiO_2–ZnO: Al seed layer (photo-anode) crystals.

Instruments

Characterization was conducted using the Bruker Quantax X-Flash for Energy Dispersive X-ray Spectroscopy (EDX) testing and the Perkin Elmer Spectrum Two FT-IR Spectrometer for Fourier Transform Infrared (FTIR) analysis. Sample composition was determined *via* energy-dispersive X-ray (EDX) testing, which involves using X-rays to analyze the elemental composition of materials. The purpose of EDX testing is to determine the composition of a sample by providing information about the elements present. These analyses were conducted at an accelerating voltage of 10 kV and a magnification of 1.300 × with an analysis time of 5 minutes.

The FTIR (Fourier-transform infrared spectroscopy) test was carried out on dyes to determine chemical bonds in natural dyes. In this case, testing was performed explicitly on dyes to identify and analyse chemical bonds found in natural dyes. Experiments were conducted on spectra collected through the total attenuation reflectance (ATR) method, ranging from 400 cm^{-1} to 4000 cm^{-1} and resolution of 4 cm^{-1}.

DSSC fabrication

Cells were arranged to form a sandwich structure consisting of a working electrode (FTO covered with TiO_2–ZnO and aluminium doped and immersed in a dye solution), electrolyte, and counter electrode. The electrolyte was-prepared by dissolving 8.3 g of KI and 1.26 g of I_2 into 100 mL of Polyethylene Glycol (PEG). The counter electrode was produced by coating grafit on top of the FTO until it was evenly distributed over the entire surface. The FTO glass containing TiO_2–ZnO: Al + dye was then glued to the counter electrode and coated with carbon using a clamp (paper clip). The electrolyte-solution was injected through the gap between the two FTO glass plates. The DSSC test used a halogen lamp as the photon light source with an intensity ranging from 328 to 580 lux, an active area of 1 cm², and the anode was sensitized for 15 minutes.

Determination of Band Gap Energy

To calculate the band gap energy value in TiO_2–ZnO: Al + chlorophyll and TiO_2–ZnO: Al + porphyrin composite, the Tauc Plot method [33] was carried out in several calculation steps until band gap energy was obtained. The process begins with the use of the Tauc's relation formula is as follows in Eq.(1).

$$\alpha h\nu = B\,(h\nu - Eg)^{\gamma} \quad (1)$$

where: α - 2.302 A;
$h\nu$ - $(hc)/\lambda$ or Eg;
A - the absorbance (arbitrary units, au);
B - a constant;
Eg - the band gab (eV);
H - Planck's constant, $6{,}626\times10^{-34}$ J.s or 4.14125×10^{-15} eV.s (where 1 eV=1.6×10^{-19} J);
ν - a frequency (equivalent to $\frac{c}{\lambda}$; where c is 3×10^{8} m/s and= wavelength obtained in nm);
γ - ½ for direct type semiconductors;
λ - the wavelength (nm).

Current and voltage measurement

Current and voltage measurements were taken to determine photovoltaic parameters: *Isc* and *Vsc*. The Fill Factor (*FF*) was calculated according to the following Eqs.(2,3) [34-37].

$$FF = \frac{I_{max}\times V_{max}}{I_{sc}\times V_{sc}} \quad (2)$$

$$\eta = \frac{FF\times I_{sc}\times V_{sc}}{P_{in}}\times 100\% \quad (3)$$

where: V_{max} - the maximum voltage (mV);
V_{sc} -the open-circuit voltage (mV);
I_{max} - the maximum current (μA cm^{2});
I_{sc} -the short-circuit current (μA cm^{-2});
P_{max} - the total power (W/cm^2);
P_{in} - the power of the halogen lamp (W/cm^2, 479×10^{-7} W/cm^2 to 846.9×10^{-7} W/cm^2).

Results and discussion

Absorbance measurements were conducted using an ultraviolet-visible (UV-Vis) spectrometer

The optical properties of the composites were characterized by generating absorbance data with the UV-Vis spectrometer. Calculations to determine the band gap energy (*Eg*) were performed using the Tauc Plot method. The characterization of TiO_2 composites with Al-doped ZnO was carried out over a wavelength range of 300–800 nm, spanning from ultraviolet to visible light.

Figure 1 illustrates the variations in absorbance at different wavelengths. The TiO_2 composite with Al-doped ZnO exhibits the highest absorbance at a wavelength of 530 nm, with a value of 1.44 a.u. The same composite shows the lowest absorbance at the same wavelength, with a value of 1.0175 a.u.

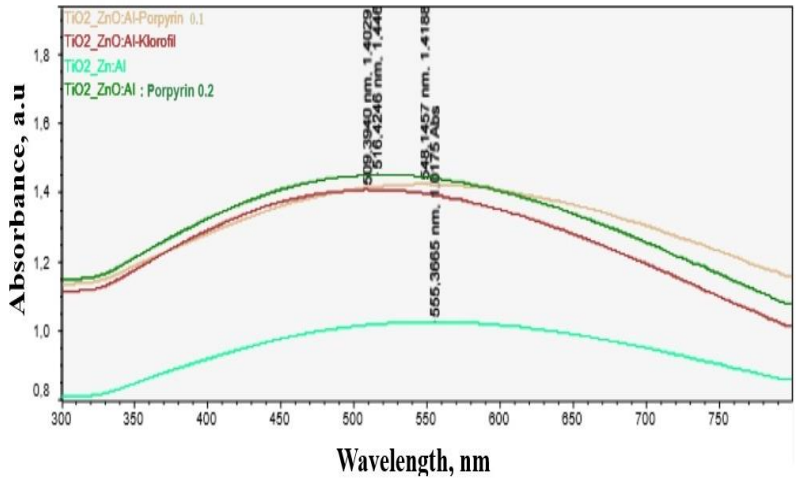

Figure 1. Graph showing the relationship between wavelength and absorbance for various composite variations.

Variations in composites containing dyes from chlorophyll and porphyrin exhibit absorbance values close to those of the TiO_2 composite with Al-doped ZnO. Absorbance decreases at wavelengths below 500 nm and above 550 nm. These changes indicate differing optical absorption properties in each sample, which affect the band gap energy values.

Band Gap Energy

The energy difference between the valence band and the conduction band in a semiconductor material. It determines the wavelength of light the material can absorb. By plotting $(\alpha\ Eg)^2$ against *Eg*, a linear relationship is expected for direct band-gap materials. The intercept on the energy axis (*Eg* axis) can be used to determine the band-gap energy.

Figure 2 illustrates that the largest band gap energy (*Eg*) occurs in the TiO_2 composite with Al-doped ZnO and Porphyrin 0.2, which is 1.25 eV. Conversely, the smallest band gap is found in the TiO_2 composite with Al-doped ZnO and Porphyrin 0.1 dye, measuring 1.1 eV. The data indicate that Al doping effectively reduces the band gap energy of TiO_2, which originally was 3.2 eV [38], and ZnO, originally 3.7 eV [39]. Furthermore, the band gap of Al-doped ZnO itself is recorded at 3.24 eV [40]. This reduction is more pronounced when ZnO: Al is composited with TiO_2. Importantly, a decrease in the band gap enhances light absorption, thereby improving the performance of solar cells. Based on these findings, this alternative material TiO_2 with Al-doped ZnO and porphyrin dye shows to be promising.

Aluminium (Al) doping offers benefits because Al acts as an electron acceptor, reducing the recombination rate of electron-hole pairs. Furthermore, Al doping enhances the absorption spectrum from 400−800 nm, facilitating charge transfer from the interior to the surface of the TiO_2 [41]. Doping TiO_2 with anionic species such as Al introduces a type of anion doping, where the combination of the doped anion's p orbitals (*e.g.*, from N or Si) with the O_{2p} orbitals of TiO_2 elevates the valence band and lowers the band gap of the photo-catalyst.

FTIR characteristics

FTIR is a test to determine the functional groups formed in the DSSC layer. Figures S1-3 (in Supplementary material) show the results of the FTIR test of TiO_2–ZnO: Al with chlorophyll dye porphyrin (2:2:0.1) and porphyrin (2:2:0.2), respectively. The test results show several functional groups at specific wave numbers with wave crests formed. There is an absorption spectrum indicating the presence of anthocyanins with a range of 3200–3400 cm^{-1}, namely 3347 cm^{-1} (chlorophyll), 3267 cm^{-1} (porphyrin 2:2:0.1), and 3341 cm^{-1} (porphyrin 2:2:0.2) [42].

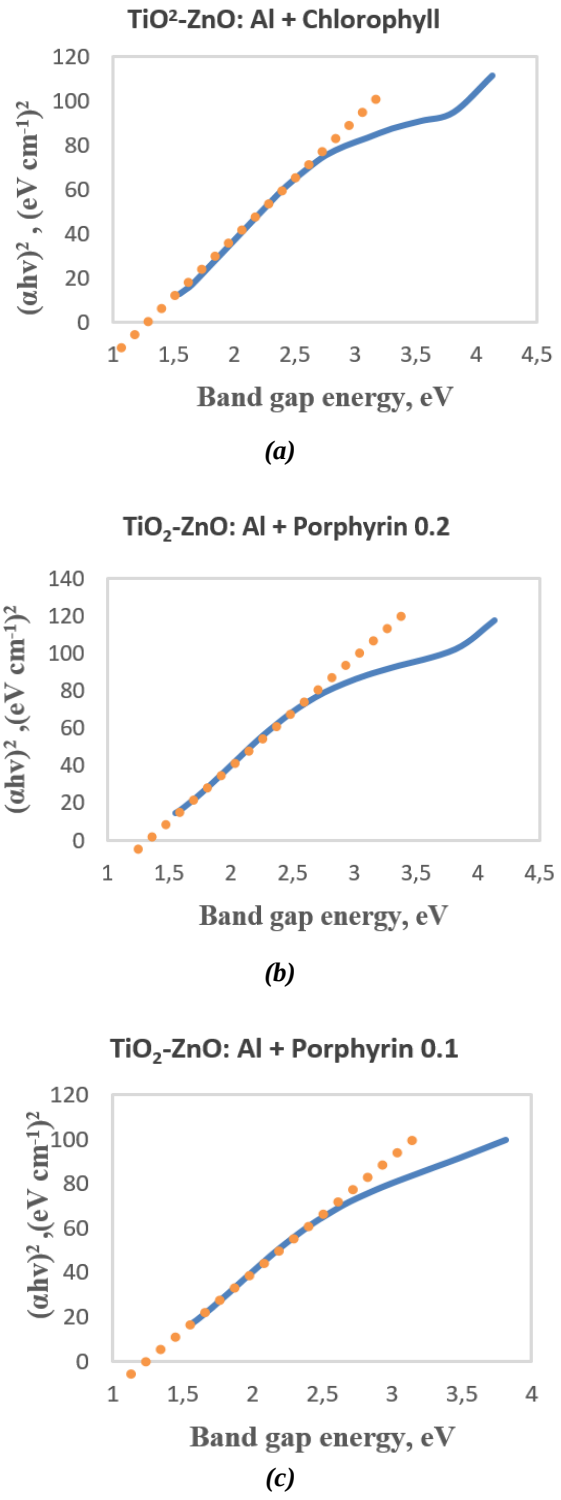

Figure 2. Determination of band gap energy of TiO_2-ZnO: Al Composites with Chlorophyll *(a)*, Porphyrin 0.1 c *(b)*, Porphyrin 0.2 *(c)*.

Some of the functional groups that occur can be seen in Table 1.

Absorption occurred with vigorous intensity, indicating the presence of the OH group at wave numbers 3383.26 cm^{-1} (TiO_2–ZnO: Al with dye chlorophyll), 3458.48 cm^{-1} (TiO_2–ZnO composites: Al and porphyrin (2: 2: 0.1), and 3371.68 cm^{-1} (TiO_2–ZnO composites: Al and porphyrin (2: 2: 0.2). The spectrum results also show moderate intensity absorption at a wave number of 1413.9 cm^{-1} (TiO_2–ZnO: Al with dye chlorophyll), 1398.44 cm^{-1} (TiO_2–ZnO composites: Al and porphyrin (2: 2: 0.1), and 1398.44 cm^{-1} (TiO_2–ZnO composites: Al and porphyrin (2: 2: 0.2), corresponding to C-H bonds. These functional groups align with those found in the anthocyanins framework.

Figures 3-5 depict the FTIR spectra of TiO_2 and Al-doped ZnO. The formation of hetero-junctions is observed in the 400–4000 cm^{-1} wave-number range, allowing the identification of various chemical and functional groups within the compounds. Ti–O–Ti bonds reveal the formation of TiO_2. Calcination at 250°C causes the transmission or absorption band to sharpen at 400–900 cm^{-1}, indicating the TiO_2 anatase phase.

The second-highest peak occurred at | 3850 cm^{-1} (chlorophyll), 3759 cm^{-1} (porphyrin 2:2:01), and 3711 cm^{-1} (porphyrin 2:2:02), corresponding to the O-H stretch of alcohol [40]. In the 1184 cm^{-1} band (chlorophyll), 1194 cm^{-1} (porphyrin 2:2:01), and 1198 cm^{-1} (porphyrin 2:2:02), the bending of the Ti-O-Ti mode was observed. Transmission bands at 1481 cm^{-1} (chlorophyll), 1479 cm^{-1} (porphyrin 2:2:01), and 1483 cm^{-1} (porphyrin 2:2:02) represented symmetrical strain vibrations of the carboxylate group. A peak at 1726 cm^{-1} (chlorophyll), 1734 cm^{-1} (porphyrin 2:2:01), and 1728 cm^{-1} (porphyrin 2:2:02) corresponded to the carbonyl, indicating a sol-gel reaction [45]. A peak in the 850-997 cm^{-1} range is associated with stretching the Zn–O band. Similar behaviour was observed for the three conditions, as their respective bands appeared in the 652 cm^{-1} region, easily comparable with Zn-O. At 1386–1535 cm^{-1} (chlorophyll), 1394–1568 cm^{-1} (porphyrin 2:2:01), and 1398–1560 cm^{-1} (porphyrin 2:2:02) for mixed oxides, only ZnO can create an asymmetric stretching mode in the presence of oxygen in the sample [46-49].

EDX Characteristics

EDX detects X-ray signals to produce elemental analysis. Because each element emits different characteristic X-rays, EDX detectors can differentiate and measure the essential presence and distribution in the scanned area [50]. Characterizing the DSSC layer using EDX aims to determine the elemental composition of the sample surface. Figures 3-5 and Tables 2-4 illustrate the actual content in DSSC.

From the EDX spectra, the analysis results provide data on the composition of elements present on the surface of the TiO_2–ZnO: Al photo-electrode with chlorophyll dye, along with the addition of porphyrin (2:2:0.1) and (2:2:0.2), as shown in Tables 2-4. Figures 3-5 display the EDX spectrum in the DSSC layer with elemental composition.

Table 2 illustrates percentages such as 20.61% for Ti K, 63.44% for O K, 1.47% for Zn K, and 0.87% for Al K.

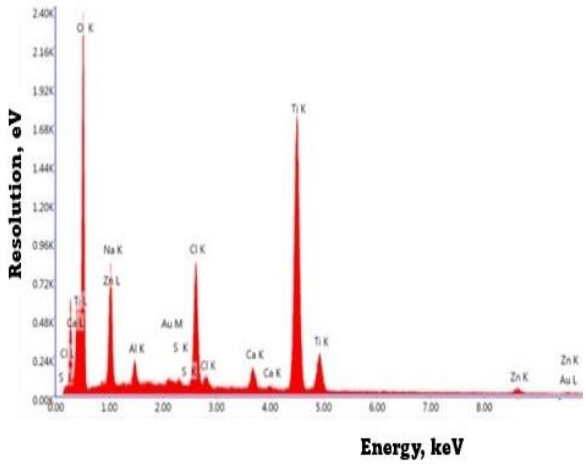

Figure 3.-EDX TiO_2-ZnO: Al with dye chlorophyll.

Table 1

Functional groups of TiO_2–ZnO: Al + chlorophyll and TiO_2–ZnO: Al + porphyrin composite [42,43].

Wavenumbers	*Functional groups*
1234.5－1238.34	vibration Ti-O-O
1614.47－1633.8	bending vibration of H_2O and Ti-OH
2351.3－2374.45	vibration CO_2
3358.23－362.04	H-OH absorbs water

Table 2

Composition of TiO_2-ZnO: Al with dye chlorophyll.

Element	*Weight (%)*	*Atomic (%)*	*Net Int.*
O K	39.91	63.44	506.73
Na K	5.8	6.42	139.21
Al K	0.92	0.87	41.47
Au M	0.63	0.08	13.68
S K	0.31	0.25	14.06
Cl K	7.52	5.39	301.81
Ca K	2.32	1.47	63.63
T_i K	38.82	20.61	837.65
Zn K	3.77	1.47	15.98

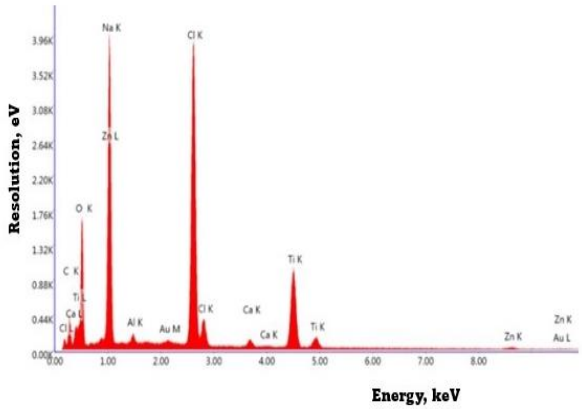

Figure 4. EDX TiO_2-ZnO: Al with dye porphyrin.

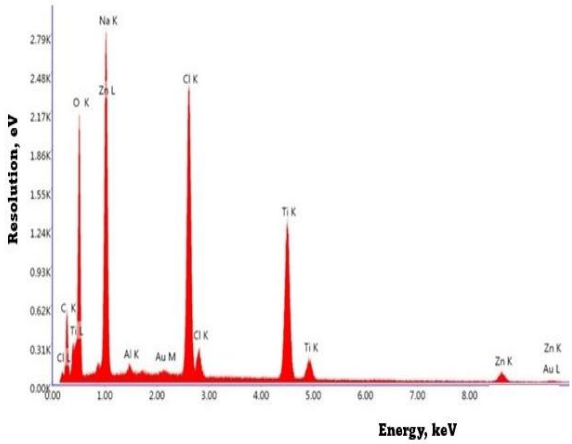

Figure 5. EDX TiO_2–ZnO: Al with dye porphyrin (2: 2: 0.2).

Table 3

Composition of TiO_2–ZnO: Al with dye porphyrin (2: 2: 0.1).

Element	*Weight (%)*	*Atomic (%)*	*Net Int.*
C K	9.93	19.75	55.75
O K	19.67	29.36	350.35
Na K	20.52	21.32	867.06
Al K	0.51	0.45	31.12
Au M	0.53	0.06	16.97
Cl K	28.2	19	1494.9
Ca K	1.08	0.65	36.79
Ti K	17.09	8.52	474.97
Zn K	2.46	0.9	13.98

Table 4

Composition of TiO_2–ZnO: Al with dye porphyrin (2: 2: 0.2).

Element	*Weight (%)*	*Atomic (%)*	*Net Int.*
C K	13.52	25.67	102.66
O K	25.06	35.72	453.07
Na K	14.27	14.16	539.21
Al K	0.19	0.16	11.04
Au M	0.28	0.03	8.21
Cl K	17.65	11.36	927.58
Ti K	21.79	10.38	613.13
Zn K	7.24	2.53	40.35

Table 3 continues with percentages like 8.52% for Ti K, 29.36% for O K, 0.9% for Zn K. Table 4 illustrates the composition of TiO_2-ZnO: Al with dye porphyrin (2:2:0.2), showcasing percentages such as 10.38% for Ti K, 35.72% for O K, 2.53% for Zn K, 25.67% for C K, and 0.16% for Al K. The elements Ti, Zn, Al, and O indicate the formation of TiO_2 and ZnO compounds, which aligns with previous studies [51,52]. Additionally, elements C, K, and Ca in chlorophyll and Na and Cl are identified as elements found in FTO glass.

The C and O elements in TiO_2 act as electron transfer connectors within its porous structure. Compounds of carbon in the hexagonal three-electron layer form covalent bonds with neighboring carbon atoms. The fourth electron acts as a free electron that moves across the coating's surface, enabling the conduction of electric currents. Element O, as an electron acceptor, captures the electrons generated from the dye. In the presence of elemental C, O, and P in TiO_2, the charge of the dye can be captured by the molecules of C, O, and P. This charge can then be rapidly transferred to the next TiO_2 particle.

Tables 2-4 highlight the presence of elements Au, Ca, Cl, K, Mg, Na, O, and S. Ca, K, S, and Mg that are essential elements in chlorophyll, with the used chlorophyll originating from *Syzygium Paniculatum*, a plant belonging to the Myrtaceae family. The Na element is derived from the NaOH ligand, while Cl comes from aluminium nitrate ($AlCl_3$) as a dopant compound. The presence of gold may be attributed to contamination during sample preparation or handling.

Current-Voltage (I-V) Testing

This point on the I-V curve represents the optimal combination of current and voltage where the solar cell produces maximum power. The coordinates of the Maximum Power Point are often denoted as (*Imp*, *Vmp*).

Measurement of the I-V Curve

The current-voltage (I-V) curve measurement is a crucial method for estimating the power conversion efficiency of solar cells. The speed of voltage scanning (vs) may induce a capacitive current depending on the cell's capacitance, potentially affecting the shape of the I-V curve. S-shaped I-V characteristics are common challenges in the development of new solar cell materials and device architectures [53]. These characteristics typically indicate a charge transport bottleneck, often at one of the selective contact layers. Overcoming this bottleneck through interface engineering and doping is essential for achieving high fill factors and enhancing power

conversion efficiencies [54]. For I-V curves, the maximum power point significantly shifts toward lower voltages, as illustrated in Figure 6.

The smallest fill factor (*FF*) values were observed when using the method proposed in this paper, in comparison to those presented in [55]. Additionally, the proposed method achieves an excellent match between the measured and estimated curves, as demonstrated in Table 5.

DSSC Performance Metrics

Current, voltage, and efficiency measurements are crucial for evaluating the performance of each DSSC, as depicted in Table 5. The performance of DSSCs relies on parameters, such as short-circuit current (I_{sc}), open-circuit voltage (V_{oc}), fill factor (*FF*), and energy conversion efficiency (η). The efficiency of DSSCs was assessed by incorporating dyes (chlorophyll, porphyrin 2:2:0.1, and porphyrin 2:2:0.2) and analysing the current-voltage (I-V) curves under halogen lamp irradiation. Table 5 shows that the DSSC with added chlorophyll achieved the highest values for I_{sc} (269.3 μA), V_{oc} (78 mV), and efficiency (13.32%). The addition of porphyrin 2:2:0.2 resulted in an I_{sc} of 212.6 μA, V_{oc} of 105 mV, and an efficiency of 13.95%. The improved performance in DSSCs are attributed to the addition of dyes, which facilitate electron transfer by acting as bridges between the porous TiO_2 and ZnO: Al molecules, thus reducing barriers in the electron transfer process [56]. This study achieved efficiencies surpassing those of non-ruthenium research using I_2/I_3^- electrolytes, which reported an efficiency of 11.5% [57].

This phenomenon shortens the charge delivery distance, leading to increased electric current and improved DSSC performance.

Table 5

Performance of DSSC.

Photo-electrode and dye	V_{sc} *(mV)*	I_{sc} *(μA)/cm²*	V_{max} *(mV)*	I_{max} *(μA)/cm²*	*FF*	$P_{max} \times 10^9$ *(W/cm²)*	$P_{in} \times 10^7$ *(W/cm²)*	η *(%)*
TiO_2–ZnO: Al and chlorophyll	53	269.3	45.0	163.7	0.516	7364.8	777.4	9.47
	72	266.9	58.5	172.1	0.524	10069.6	821.3	12.3
	58.4	262.1	46.1	177.9	0.536	8204.4	825.7	9.9
	42.2	257.4	29.5	192.0	0.521	5664.0	834.5	6.8
	78	193.7	69.3	160.0	0.733	11074.6	831.6	13.3
TiO_2–ZnO: Al and porphyrin (2:2:0.1)	28.3	276.3	20.0	197.1	0.504	3946.3	833.0	4.7
	32.5	276.2	21.1	189.0	0.444	3985.6	775.9	5.1
	40.2	278.4	22.1	198.1	0.391	4375.9	846.2	5.2
	37	278.1	22.3	238.0	0.516	5309.5	620.7	8.6
	38.6	278.7	23.4	238.5	0.518	5572.6	625.1	8.9
TiO_2–ZnO: Al and porphyrin (2:2:0.2)	47	111.7	29.5	83	0.472	2477.9	412.9	6
	42	152.9	32.0	85	0.424	2722.8	420.2	6.5
	54	212.6	46.6	87	0.353	4054.2	761.4	5.3
	97	132.5	92.9	86	0.662	7994.3	790.6	10.1
	105	87.2	96.0	69.6	0.730	6683.9	479.0	13.9

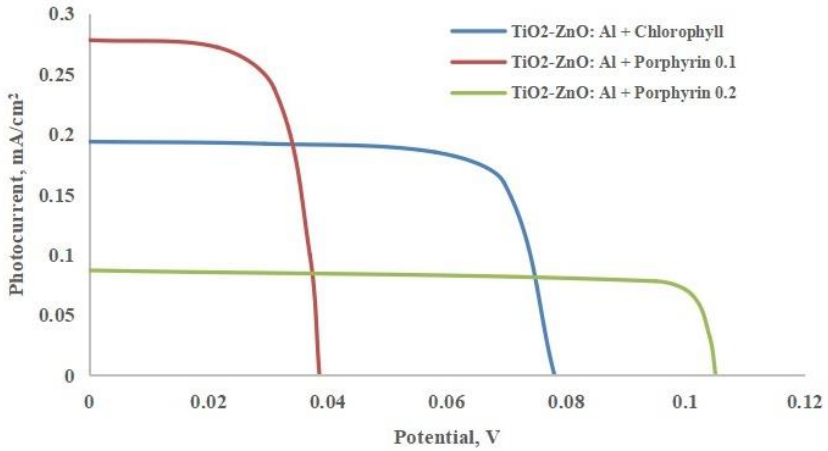

Figure 6. Series of I–V curves.

Conclusion

The integration of natural dyes (chlorophyll and porphyrin) into DSSC was successfully achieved. Adding dye to the composite fills voids between TiO_2–ZnO: Al molecules, decreasing gaps and accelerating electron transfer, ultimately reducing electron recombination rates. The study reveals that incorporating dye into TiO_2–ZnO: Al enhances DSSC performance, showcasing optimal characteristics in absorptivity, optical band gap, and electrical parameters. The highest DSSC efficiency achieved is 13.95%, emphasizing the interdependence of absorbent layer quality with photovoltaic performance.

Acknowledgments

The Research Unit of Politeknik Negeri Bandung funded this research.

Supplementary information

Supplementary data are available free of charge at http://cjm.ichem.md as PDF file.

References

1. Gratzel, M. Solar energy conversion by dye-sensitized photovoltaic cells. Inorganic Chemical, 2005, 44(20), pp. 6841–6851. DOI: https://doi.org/10.1021/ic0508371
2. Nazeeruddin, M.K.; De Angelis, F.; Fantacci, S.; Selloni, A.; Viscardi, G.; Liska, P.; Ito, S.; Takeru, B.; Grätzel, M. Combined experimental and DFT-TDDFT computational study of photoelectrochemical cell ruthenium sensitizers. Journal of the American Chemical Society, 2005, 127(48), pp. 16835–16847. DOI: https://doi.org/10.1021/ja052467l
3. Yella, A.; Lee, H.W.; Tsao, H.N.; Yi, C.; Chandiran, A.K.; Nazeeruddin, M.K.; Diau, E.W.-G.; Yeh, C.-Y.; Zakeeruddin, Z.M.; Grätzel, M. Porphyrin-sensitized solar cells with cobalt (II/III)—based redox electrolyte exceed 12 percent efficiency. Science, 2011, 334(6056), pp. 629–634. DOI: https://doi.org/10.1126/science.1209688
4. Mathew, S.; Yella, A.; Gao, P.; Humphry-Baker, R.; Curchod, B.F.E.; Ashari-Astani, N.; Tavernelli, I; Rothlisberger, U.; Nazeeruddin, M.K.; Gratzel, M. Dye-sensitized solar cells with 13% efficiency achieved through the molecular engineering of porphyrin sensitizers. Nature Chemistry, 2014, 6, pp. 242–247. DOI: https://doi.org/10.1038/nchem.1861
5. Akila, Y.; Muthukumarasamy, N.; Velauthapillai, D. TiO_2-based dye-sensitized solar cells. Nanomaterials for Solar Cell Applications, 2019, pp. 127–144. DOI: https://doi.org/10.1016/B978-0-12-813337-8.00005-9
6. Kenji, T.; Hisahiro, E. Distribution ratio of Pt on anatase and rutile TiO_2 particles, determined by X-ray diffraction and transmission electron microscopy analysis of Pt/TiO_2 (P25). Evergreen, 2018, 5(4), pp. 13–17. DOI: https://doi.org/10.5109/2174853
7. Hussein, A.M.; Iefanova, A.; Koodali, R.T.; Logue, B.A.; Shende, R.V. Interconnected ZrO_2 doped ZnO/TiO_2 network photoanode for dye-sensitized solar cells. Energy Reports, 2018, 4, pp. 56–64. DOI: https://doi.org/10.1016/j.egyr.2018.01.007
8. Dwirekso, I.H.; Muhammad, I.; Slamet Synthesis of TiO_2-SiO_2-CuO nanocomposite material and its activities for self-cleaning. Evergreen, 2020, 7(2), pp. 285–291. DOI: https://doi.org/10.5109/4055234
9. González-Verjan, V.A.; Trujillo-Navarrete, B.; Félix-Navarro, R.M.; Díaz de León, J.N.; Romo-Herrera, J.M.; Calva-Yáñez, J.C.; Hernández-Lizalde, J.M.; Reynoso-Soto, E.A. Effect of TiO_2 particle and pore size on DSSC efficiency. Materials for Renewable and Sustainable Energy, 2020, 9, 13, pp. 1–8. DOI: https://doi.org/10.1007/s40243-020-00173-7
10. He, X.; Zhang, J.; Guo, Y.; Liu, J.; Li, X. Hierarchical TiO_2 microspheres composed with nanoparticle-decorated nanorods for the enhanced photovoltaic performance in dye-sensitized solar cells. RSC Advances, 2019, 9(6), pp. 3056–3062. DOI: https://doi.org/10.1039/C8RA09145E
11. Arifin, Z.; Hadi, S.; Suyitno; Sutanto, B.; Widhiyanuriyawan, D. Investigation of curcumin and chlorophyll as mixed natural dyes to improve the performance of dye-sensitized solar cells. Evergreen, 2022, 9(1), pp. 17–22. DOI: https://doi.org/10.5109/4774212
12. Ramya, M.; Nideep, T.K.; Nampoori, V.P.N.; Kailasnath, M. Solvent assisted evolution and growth mechanism of zero to three dimensional ZnO nanostructures for dye-sensitized solar cell applications. Scientific Reports, 2021, 11, 6159, pp. 1–15. DOI: https://doi.org/10.1038/s41598-021-85701-9
13. Vittal, R.; Ho, K.-C. Zinc oxide-based dye-sensitized solar cells: A review. Renewable and Sustainable Energy Reviews, 2017, 70, pp. 920–935. DOI: https://doi.org/10.1016/j.rser.2016.11.273
14. Cho, S.II; Sung, H.K.; Lee, S.J.; Kim, W.H.; Kim, D.H.; Han, Y.S. Photovoltaic performance of dye-sensitized solar cells containing ZnO microrods. Nanomaterials, 2019, 9(12), 1645, pp. 1–12. DOI: https://doi.org/10.3390/nano9121645
15. Fauzi, A.; Lalasari, L.H.; Sofyan, N.; Ferdiansyah, A.; Dhaneswara, D.; Yuwono, A.H. Titanium dioxide nanosheets derived from Indonesian ilmenite mineral through post-hydrothermal process. Evergreen, 2022, 9(2), pp. 470–475. DOI: https://doi.org/10.5109/4794174
16. Anta, J.A; Guillén, E.; Tena-Zaera, R. ZnO-based dye-sensitized solar cells. The Journal of Physical Chemistry C, 2012, 116(21), pp. 11413–11425. DOI: https://doi.org/10.1021/jp3010025
17. Lin, S.; Hu, H.; Zheng, W.; Qu, Y.; Lai, F. Growth and optical properties of ZnO nanorod arrays on Al-doped ZnO transparent conductive film. Nanoscale Research Letters, 2013, 8, 158, pp. 1–6. DOI: https://doi.org/10.1186/1556-276X-8-158
18. Pujiarti, H.; Pangestu, Z.A.; Sholeha, N.; Nasikhudin, N.; Diantoro, M.; Utomo, J.;

Aziz, M.S.A. The effect of Acetylene Carbon Black (ACB) loaded on Polyacrylonitrile (PAN) nanofiber membrane electrolyte for DSSC applications. Micromachines, 2023, 14(2), 394, pp. 1–12. DOI: https://doi.org/10.3390/mi14020394
19. Fuchs, P.; Hagendorfer, H.; Romanyuk, Y.E.; Tiwari, A.N. Doping strategies for highly conductive Al-doped ZnO films grown from aqueous solution. Physica Status Solidi, 2015, 212(1), pp. 51–55. DOI: https://doi.org/10.1002/pssa.201431145
20. Kaur, G.; Mitra, A.; Yadav, K.L. Pulsed laser deposited Al-doped ZnO thin films for optical applications. Progress in Natural Science, 2015, 25(1), pp. 12–21. DOI: https://doi.org/10.1016/j.pnsc.2015.01.012
21. Dwivedi, S.P.; Maurya, M.; Maurya, N.K.; Srivastava, A.K.; Sharma,S.; Saxena, A. Utilization of groundnut shell as reinforcement in development of aluminum based composite to reduce environment pollution: a review. Evergreen, 2020, 7(1), pp. 15–25. DOI: https://doi.org/10.5109/2740937
22. Rini, A.S.; Rati, Y.; Fadillah, R.; Farma, R.; Umar, L.; Soerbakti, Y. Improved photocatalytic activity of ZnO film prepared via green synthesis method using red watermelon rind extract. Evergreen, 2022, 9(4), pp. 1046–1055. DOI: https://doi.org/10.5109/6625718
23. Sanchez, H.E.; Esparza, D.; Lopez-Luke, T.; Castañeda-Contreras, J.; Marañon-Ruiz, V.F.; Zarazúa, I.; Rodriguez, R.A. Effect of Al^{3+} doping concentration and film thickness of ZnO nanoparticles over the TiO_2 photoelectrode in CdS quantum dots sensitized solar cells. Solar Energy, 2020, 197, pp. 154–162. DOI: https://doi.org/10.1016/j.solener.2019.12.023
24. Dyartanti, E.R.; Widiasa, I.N.; Purwanto, A.; Susanto, H. Nanocomposite polymer electrolytes in PVDF/ZnO membranes modified with PVP for use in $LiFePO_4$ batteries. Evergreen, 2018, 5(2), pp. 19–25. DOI: https://doi.org/10.5109/1936213
25. Zhang, L.; Zhang, J.; Liu, Y.; Zheng, P.; Yuan, X.; Guo, S. Al doped-ZnO nanoparticles implanted in reduced graphene oxide with improved electrochemical properties for lithium ion batteries. Materials Letters, 2016, 165, pp. 165–168. DOI: https://doi.org/10.1016/j.matlet.2015.12.007
26. Chou, J.-C.; Ko, C.-C.; Chang, J.-X.; Lai, C.-H; Nien, Y.-H.; Kuo, P.-Y.; Chen, H.-H.; Hsu, H.-H.; Hu, G.-M. Dye-sensitized solar cells using aluminum-doped zinc oxide/titanium dioxide photo anodes in parallel. Energies, 2019, 12(18), 3469, pp. 1–13. DOI: https://doi.org/10.3390/en12183469
27. García-Salinas, M.J.; Ariza, M.J. Optimizing a simple natural dye production method for dye-sensitized solar cells: examples for betalain (bougainvillea and beetroot extracts) and anthocyanin dyes. Applied Sciences, 2019, 9(12), 2515, pp. 1–20. DOI: https://doi.org/10.3390/app9122515
28. Tsay, C.-Y.; Yu, S.-H. Melioration of electrical and optical properties of Al and B Co-doped ZnO transparent semiconductor thin films. Coatings, 2021, 11(10), 1259, pp. 1–12. DOI: https://doi.org/10.3390/coatings11101259
29. Sarfraz, M.; Ahmed, N.; Khizar, U.-H.; Shahida, S.; Khan, M.A. Structural optical and magnetic properties of transition metal doped ZnO magnetic nanoparticles synthesized by sol-gel auto-combustion method. Materials Science-Poland, 2019, 37(2), pp. 280–288. DOI: https://doi.org/10.2478/msp-2019-0029
30. Idris, A.S.; Ghosh, S.; Jiang, H.; Hamamoto, K. A multi-layer stacked all sol-gel fabrication technique for vertical coupled waveguide. Evergreen, 2017, 4(2/3), pp. 12–17. DOI: https://doi.org/10.5109/1929657
31. Toghan, A.; Taha, K.K.; Modwi, A. TiO_2–ZnO composites fabricated via sonication assisted with gelatin for potential use in rhodamine B degradation. Journal of Materials Science: Materials in Electronics, 2021, 32, pp. 2471–2485. DOI: https://doi.org/10.1007/s10854-020-05013-y
32. Ungan, H.; Tekin, T. Effect of the sonication and coating time on the photocatalytic degradation of TiO_2, TiO_2-Ag, and TiO_2-ZnO thin film photocatalysts. Chemical Engineering Communications, 2020, 207(7), pp. 896-903. DOI: https://doi.org/10.1080/00986445.2019.1630395
33. Makula, P.; Pacia, M.; Macyk, W. How to correctly determine the band gap energy of modified semiconductor photocatalysts based on UV−Vis spectra. The Journal of Physical Chemistry Letters, 2018, 9(23), pp. 6814−6817. DOI: https://doi.org/10.1021/acs.jpclett.8b02892
34. Varghese, O.K.; Grimes, C.A. Appropriate strategies for determining the photoconversion efficiency of water photoelectrolysis cells: A review with examples using titania nanotube array photoanodes. Solar Energy Materials and Solar Cells, 2008, 92(4), pp. 374–384. DOI: https://doi.org/10.1016/j.solmat.2007.11.006
35. Bartesaghi, D., Pérez, I., Kniepert, J.; Roland, S.; Turbiez, M.; Neher, D.; Koster, L.J.A. Competition between recombination and extraction of free charges determines the fill factor of organic solar cells. Nature Communications, 2015, 6, 7083, pp. 1–10. DOI: https://doi.org/10.1038/ncomms8083
36. Muhammad, F.F.; Yahya, M.Y.; Hameed, S.S.; Aziz, F.; Sulaiman, K.; Rasheed, M.A.; Ahmad, Z. Employment of single-diode model to elucidate the variations in photovoltaic parameters under different electrical and thermal conditions. Plos One, 2017, 12(8), e0182925, pp. 1–20. DOI: https://doi.org/10.1371/journal.pone.0182925
37. Wuryanti, S. The performance of solar cells using chlorophyll dye from *Syzygium paniculatum*. Clean Energy, 2021, 5(3), pp. 433-440. DOI: https://doi.org/10.1093/ce/zkab022
38. Pawar, M.; Topcu Sendoğdular, S.; Gouma, P. A brief overview of TiO_2 photocatalyst for organic dye

remediation: case study of reaction mechanisms involved in Ce-TiO_2 photocatalysts system. Journal of Nanomaterials, 2018, pp. 1–13. DOI: https://doi.org/10.1155/2018/5953609
39. Rafiee, Z.; Roshan, H.; Sheikhi, M.H. Low concentration ethanol sensor based on graphene/ZnO nanowires. Ceramics International, 2021, 47(4), pp. 5311–5317. DOI: https://doi.org/10.1016/j.ceramint.2020.10.111
40. Sugianto, S.; Astuti, B.; Marwoto, P.; Firmahaya, N.A.; Aryanto, D.; Isnaeni. Influence of annealing duration on structural, optical and electrical properties of AZO thin films grown on corning glass by dc magnetron sputtering. Journal of Physics: Conference Series, 2020, 1567, 022003, pp. 1–6. DOI: https://doi.org/10.1088/1742-6596/1567/2/022003
41. Pambudi. A.B.; Kurniawati, R.; Iryani, A.; Hartanto, D. Effect of calcination temperature in the synthesis of carbon doped TiO_2 without external carbon source. AIP Conference Procedings, 2018, 2049(1), 020074, pp. 1–5. DOI: https://doi.org/10.1063/1.5082479
42. Jaffar, H.A.; Ismaeel, A.A.; Shuraiji, A.L. Review of hybrid photovoltaic - air updraft solar application: present and proposed state models. Evergreen, 2022, 9(4), pp. 1181–1202. DOI: https://doi.org/10.5109/6625729
43. Gomesh, N.; Syafinar, R.; Dayang, S.; Irwanto, M.; Yeap, G.H. FT-IR and electrical characteristic of dye-sensitized solar cell using dyes from hibiscus and bougainvillea. IEEE International Conference on Power and Energy (PECon), 2016, pp. 648–651. DOI: https://doi.org/10.1109/PECON.2016.7951640
44. Li, B.; Luo, L.; Xiao, T.; Hu, X.; Lu, L.; Wang, J.; Tang, Y. Zn_2SnO_4–SnO_2 heterojunction nanocomposites for dye-sensitized solar cells. Journal of Alloys and Compounds, 2011, 509(5), pp. 2186–2191. DOI: https://doi.org/10.1016/j.jallcom.2010.10.184
45. He, X.; Wu, T.; Liu, X.; Wang, Y.; Meng, X.; Wu, J.; Noda, T.; Yang, X.; Moritomo, Y.; Segawa, H.; Han, L. Highly efficient tin perovskite solar cells achieved in a wide oxygen concentration range. Journal of Materials Chemistry A, 2020, 8(5), pp. 2760–2768. DOI: https://doi.org/10.1039/c9ta13159k
46. Chen, X.; Wang, K.; Beard, M.C. Ultrafast probes at the interfaces of solar energy conversion materials. Physical Chemistry Chemical Physics, 2019, 21(30), pp. 16399–16407. DOI: https://doi.org/10.1039/c9cp02768h
47. Haider, A.J; Jameel, Z.N.; Taha, S.Y. Synthesis and characterization of TiO_2 nanoparticles via sol-gel method by pulse laser ablation. Engineering and Technology Journal, 2015, 33(5B), pp. 761–771. DOI: https://doi.org/10.30684/etj.33.5B.1
48. Tractz, G.T; Maia, G.A.R.; Dias, B.V.; I gnachewski, F.; Rodrigues, P.R.P. Evaluation of adsorption and electrochemical study of solar cells produced with TiO_2 and dye extracted from hibiscus. Química Nova, 2018, 41(5), pp. 512–518. DOI: https://dx.doi.org/10.21577/0100-4042.20170212 (in Portuguese).
49. Gonçalves, C.L.; Corazza, M.L; Oliveira, M.M.; Rangel, J.H.G.; Vasconcelos, J.S.; de Figueredo, G.P.; Longo, E. Synthesis, and characterization of SnO_2Nb catalysts supported on Maranhão clay. Matéria, 2018, 23(1), pp. 1–11. DOI: https://dx.doi.org/10.1590/S1517-707620170001.0308
50. Rajendran, S.P.; Sengodan, K. Synthesis and characterization of zinc oxide and iron oxide nanoparticles using *Sesbania grandiflora* leaf extract as reducing agent. Journal of Nanoscience, 2017, 8348507, pp. 1–7. DOI: https://doi.org/10.1155/2017/8348507
51. Abd Mutalib, M.; Rahman, M.A.; Othman, M.H.D.; Ismail, A.F.; Jaafar, J. Scanning electron microscopy (SEM) and energy-dispersive X-ray (EDX) spectroscopy. Membrane Characterization, 2017, pp. 161–179. DOI: https://doi.org/10.1016/B978-0-444-63776-5.00009-7
52. Osayemwenre, G.O.; Meyer, E.L.; Mamphweli, S. SEM analysis as a diagnostic tool for photovoltaic cell degradation. Digest Journal of Nanomaterials and Biostructures, 2015, 10(2), pp. 479–487. https://www.chalcogen.ro/479_Osayemwenre.pdf
53. Saive, R. S-shaped current–voltage characteristics in solar cells: a review. IEEE Journal of Photovoltaics, 2019, 9(6), pp. 1477–1484. DOI: https://doi.org/10.1109/JPHOTOV.2019.2930409
54. Khan, F.; Rasheed J., F.; Alshahrani, T.; Kashif, A.S.; Alanazi, A.M.; Alsehli, A.H.; Alsowayigh, M.M.; Elamin Ahmed, N. Investigations on performance parameters of graphene interfacial layer modified $FASnI_3$: Zn-based lead-free perovskite solar cells. Materials Science and Engineering B, 2024, 301, 117209. DOI: https://doi.org/10.1016/j.mseb.2024.117209
55. Sahu, M.; Reddy, V.R.M.; Kim, B.; Patro, B.; Park, C.; Kim, W.K.; Sharma, P. Fabrication of Cu_2ZnSnS_4 light absorber using a cost-effective mechanochemical method for photovoltaic applications. Materials, 2022, 15(5), 1708, pp. 1–7. DOI: https://doi.org/10.3390/ma15051708
56. Hossain, E.S.; Chelvanathan, P.; Shahahmadi, S.A.; Bais, B.; Akhtaruzzaman, M.; Tiong, S.K.; Sopian, K.; Amin, N. Fabrication of Cu_2SnS_3 thin film solar cells by sulphurization of sequentially sputtered Sn/CuSn metallic stacked precursors. Solar Energy, 2019, 177, pp. 262–273. DOI: https://doi.org/10.1016/j.solener.2018.10.081
57. Xie, Y.; Tang, Y.; Wu, W.; Wang, Y.; Liu, J.; Li, X.; Tian, H.; Zhu, W.-H. Porphyrin cosensitization for a photovoltaic efficiency of 11.5%: a record for non-ruthenium solar cells based on iodine electrolyte. Journal of the American Chemical Society, 2015, 137(44), pp. 14055–14058. DOI: https://doi.org/10.1021/jacs.5b09665